ARTICLE

JOURNAL OF UNIVERSITY OF BABYLON For ENGINEERING SCIENCES (JUBES)

Vol.31, No.3.| 2023

An Improved Single Stage Transformer-Less Multilevel Inverter Under Conventional And Advanced MPPT Algorithms for Photovoltaic Application

Esraa H. Al-fatlawi [1] **Tahani H. M. Al-Mhana**[2]

Department of Electrical Engineering / University of Babylon. Babel, Iraq

esraa.hasson.engh306@student.uobabylon.edu.iq eng.tahany.hamodi@uobabylon.edu.iq

Received:	21/2/2023	Accepted:	25/4/2023	Published:	20/5/2023

Abstract

A transformer-less single-stage, grid-connected PV system is increasingly introduced with a multilevel inverter (MLI). MLI is employed to integrate the PV system with the utility grid due to its high efficiency, low cost, smaller size and weight. However, The leakage current due to the absence of galvanic isolation is one of the drawbacks in such system. This paper investigates a single phase three level Neutral point clamped (NPC) inverter to be employed in a single stage grid connected PV system. The system is characterized with a unity power-factor and low current total harmonic distortion (THD), low voltage stress on the semiconductor switches, no shoot through problems, high reliability and efficiency. The paper proposes the improved split-inductor (ISI-NPC) inverter as an effective candidate to be employed in such transformer-less PV system. Hysteresis current control (HCC) is designed to track the inverter output current and force it to be zero in order to achieve high power quality grid power and maintain unity power factor. A conventional and advanced maximum power point tracking algorithms including perturb and observe (P&O) and artificial neural-network (ANN) are examined to ensure extracting the maximum power from the PV panel. The whole system is designed and tested in this work. A better performance is achieved under ANN approach with HCC. The results validate the ability of the ISI-NPC inverter under HCC control and artificial neural network to transfer PV maximum power to the grid with a unity power factor, high power quality, very low current THD with a 0.37% less semiconductor switches stress, and thus high reliability. Therefore, the paper highlights that ISI-NPC is considered as an effective MLI to be employed in such system.

Keywords: Neutral point clamped, Photovoltaic system (PV), Hysteresis current control, Perturb and observe algorithm, Artificial neural network, Inverter, Single stage, grid connected , Maximum power point tracking (MPPT).

مجلة جامعة بابل للعلوم الهندسية مجلة جامعة بابل للعلوم الهندسية مجلة جامعة بابل للعلوم الهندسية

ISSN: 2616 - 9916 | www.journalofbabylon.com | Journal.eng@uobabylon.edu.iq | info@journalofbabylon.com

مجلة جامعة بابل للعلوم الهندسية | مجلة جامعة بابل للعلوم الهندسية | مجلة جامعة بابل للعلوم الهندسية

ISSN: 2616 - 9916 | www.journalofbabylon.com | Journal.eng@uobabylon.edu.iq | info@journalofbabylon.com

INTRODUCTION

Power electronic converters topologies are playing important roles in many applications [1-2]. One of the most important uses of these topologies is the transformer-less photovoltaic (PV) grid-connected inverter, which has the advantages of lower cost, higher efficiency, smaller volume, and less complexity compared to its counterparts with transformer galvanic isolation.

[5-9]. In NPC inverter topology, the neutral of the power grid is linked to the converter's dc-midpoint, thus there is no leakage current, which help to overcome one of the biggest obstacles of transformer-less PV inverters. In addition to the MLI advantages which can be summarized that: display higher output voltage with the same device ratings, low harmonic distortion, limited voltage transient dv/dt, small size filter components, good system efficiency, and lower common-mode voltages. [3-6]. However, the shoot-through problem (short circuit fault) affects traditional 3L-NPC just like it does other bridge-type inverters [10]. Dead time must be established if the issue is to be avoided. Nevertheless, dead time has an effect that distorts the result. This issue can be remedied by employing coupled/split inductor topologies. The inductors in these converters are located between the lower and higher switches of the NPC leg, which can have two or three levels. This insertion eliminates the dead-time problem and offers superior defense against the shoot-through problem [11–12]. Zargari et al. [13] pioneered the use of a split inductor (SI) topology, which mitigates the inefficiency-reducing shoot-through problem inherent in traditional half-bridge converters while simultaneously increasing efficiency. Unfortunately, the bipolar modulation approach is required for this topology to function and the voltage stress on the power components is quite high. To get beyond the noted limitations of the conventional NPC inverters and the shoot through problem, A transformer-less three level Improved Split Inductor Neutral Point Clamped Inverter- (3L-ISINPCI) for PV systems is investigated. Since the proposed topology uses a large in-series filter inductance (L1+L2) to severely limit the shoot-through di/dt and does not require the addition of dead time between the commutations of switches, this leads the converter to operate reliably and efficiently. In addition, the 3L-ISINPCI also features a low leakage current, a low current Total Harmonic Distortion (THD) and a high efficiency even at modest loads. One of the most vital components of renewable energy infrastructure are photovoltaic (PV) energy conversion systems. Power electronics advancements, along with PV cell technology, energy conversion efficiency, Photovoltaic array size and the variety of control approaches for optimal power point tracking have all contributed to the PV system. The use of photovoltaic (PV) systems as a source of electrical power has exploded in popularity in recent years for several reasons: they reduce harmful emissions and noise, endless, and require no external power source. [14-16]. Yet the efficiency of the PV generator system is quite low. A maximum power point tracking (MPPT) controller is required to get the best performance out of a photovoltaic (PV) panel [15-17]. Conventional and cutting-edge MPPT strategies have been developed. Conventional methods include "perturb and observe" [18–20], "incremental conductance" [21], "hill climbing" [22], "fractional open-circuit voltage" [23], and "fractional short-circuit current" [24] are examples of more traditional approaches. On the other hand, some of the more sophisticated approaches include the use of artificial neural networks [25] and fuzzy logic techniques [26]. Subsequently, ANN's capacity to estimate unknown parameters prompted its use for MPP tracking. These networks can be efficiently deployed in the online setting after being trained off-line for non-linear mapping [27]. This paper will try to deal with the common issues and challenges in designing a single-stage grid-connected TRL-PV Inverter such as Shoot-through problem,

DC- link capacitor voltage balance, Current total harmonic distortion (THD), Voltage stress across the semiconductor device and Grid synchronization and power quality.
In transformer-less single stage grid connected PV system, a multi-level inverter is needed. To transfer the power generated by PV system to the grid.

I. PV Cell Model

PV cells consist of p-n semiconductor elements combined as a thin layer. When PV cells are exposed to light, they generate direct current as a result of electron movement. Single diode general electrical equivalent circuit of PV cells is illustrated in Figure 1 [14]

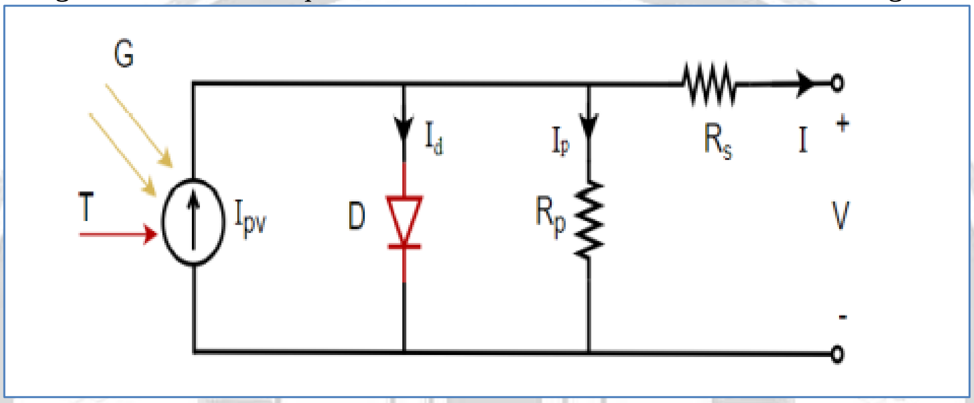

Figure 1. Equivalent circuit of cell with one diode [14]

Single diode PV cell consists of one diode (D), one current source (I_{pv}), one parallel resistor (R_p), and one series resistor (R_s). In Figure 1, the current generated by I_{pv} light photons represent the I_d diode current. Mathematical equations of the PV cell model are shown in the equations between Equation 1 and Equation 5.

$$I_{pv} - I_d - I_p - I \quad (1)$$

$$I_d = I_o\left(e^{\frac{qV_d}{kT}} - 1\right) \quad (2)$$

$$V_d = V + IR_S \quad (3)$$

$$I_d = I_o\left(e^{\frac{q(V+IR_S)}{nkT}}\right) \quad (4)$$

$$I = I_{pv} - I_o\left(e^{\frac{q(V+IR_S)}{nkT}}\right) - \frac{V+IR_S}{nkT} \quad (5)$$

Where:

I_o: reserve saturation current (A)
q: the electron charge (C),
k: is the Boltzman constant (J/K),
T: stands for the cell temperature (K) and
n: the diode idealty constant.

ISSN: 2616 - 9916 | www.journalofbabylon.com | Journal.eng@uobabylon.edu.iq | www.journalofbabylon.com | info@journalofbabylon.com

ISSN: 2616 - 9916 www.journalofbabylon.com | Journal.eng@uobabylon.edu.iq | info@journalofbabylon.com

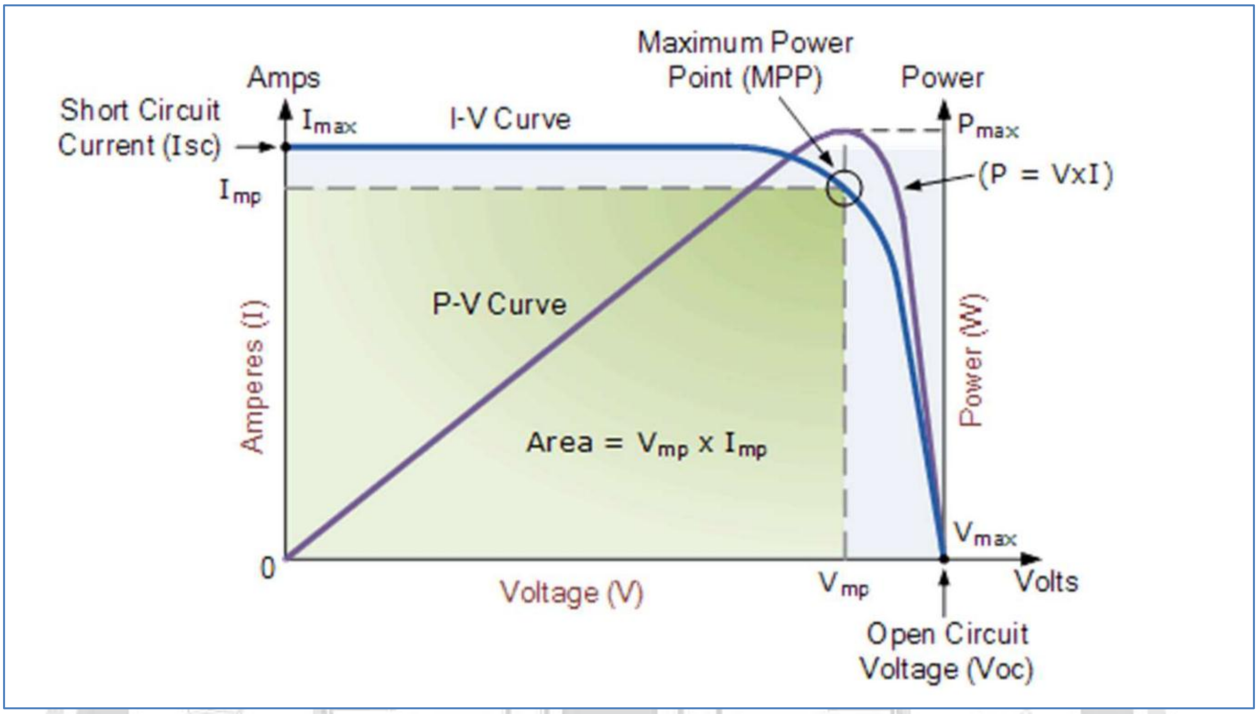

Figure 2. I-V curve and P-V curve of a PV cell

II. THREE LEVEL IMPROVED SPLIT NEUTRAL POINT CLAMPED INVERTER

The schematic representation of the three-level ISI-NPC inverter is demonstrated in Figure (3). In advance of the analysis, the following hypotheses are presented: All inductors and capacitors are perfect ($C_1 = C_2$, $L_1 = L_2 = L$), semiconductors devices (diodes and switches) are ideal, and the inverter runs at a unity power factor (the voltage at output or grid (Vg) is in phase with the current at the output (Io). [28]

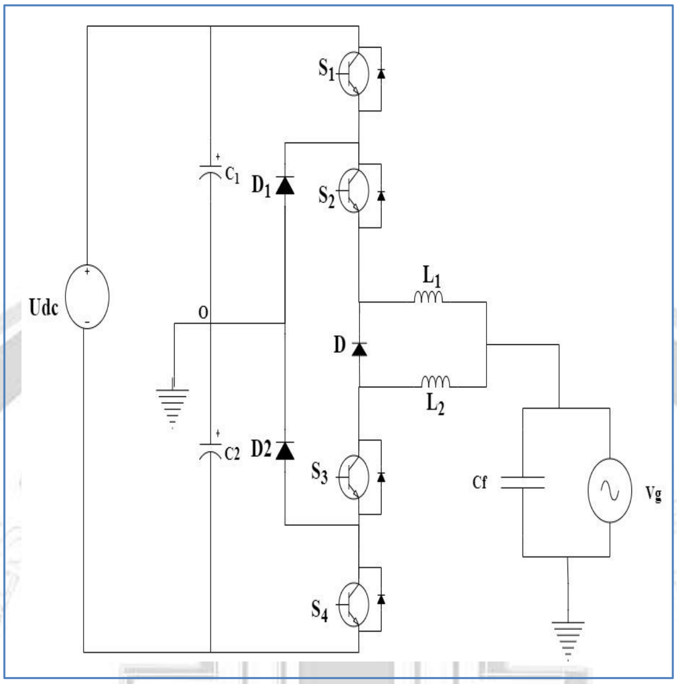

Figure 3. Three-level Improved SI-NPC [28]

In this converter the mid-point shared between two DC link capacitors and the clamping diodes. Two clamping diodes are employed D_1&D_2 to acquire the zero voltage level via mid-point. It also has a four semiconductor switches S_1, S_2, S_3, S_4 as shown in Figure (3). The upper switches S_1 and S_2 are operating in a complementary manner with the lower switches $S_3$and S_4. Split inductors (L_1 and L_2) are used to avoid the shoot through. Table (1) presents the design values of the three level Improved Split Inductor Neutral Point Clamped Multilevel inverter .

Table (1) Three level Improved Split Inductor Neutral Point Clamped Multilevel inverter components [28]

Components	Units	Value
Input voltage (Vin)	Volt	800
Capacitors (C_1=C_2)	µF	2000
Capacitor initial voltage (V_{C1} =V_{C2})	Volt	400
Inductors (L_1=L_2)	mH	4
Grid Voltage (Vg)	Volt	240

ISSN: 2616 - 9916 | www.journalofbabylon.com | Journal.eng@uobabylon.edu.iq | info@journalofbabylon.com
مـجلة جـامعة بـابل للعلـوم الهندسية

ISSN: 2616 - 9916 | www.journalofbabylon.com | Journal.eng@uobabylon.edu.iq | info@journalofbabylon.com

In this converter, three levels of the output voltage can be achieved: Vdc/2, 0 and -Vdc/2. Table (2) shows the switching state of the converter where S_1 and S_2 must remain on to obtain Vdc/2, while S_3 and S_4 must be on for - Vdc/2. Turning on either S1 and S4 or S2 and S3 will result in the same value of zero voltage level.

Table.(2) Switching states for a single-phase 3L (ISI-NPC).

Switching -state	S_1	S_2	S_3	S_4	Output Voltage
P	ON	ON	OFF	OFF	$\frac{1}{2}Vdc$
$(\pm\mathbf{0})$	OFF	ON	ON	OFF	0
N	OFF	OFF	ON	ON	$\frac{-1}{2}V_{dc}$

There are three modes of operation for 3L ISI-NPC inverter as described below:

Mode 1 [Positive, $\frac{Vdc}{2}$]: switch S_1 is on, while the switch that complements, switch S_3, is off; as a result, switch S_2 is on, while switch S_4, which complements it is off. The voltage of capacitor C_1 which is one half of supply voltage is the bridge leg's output voltage (Figure 4). During this time period the value of the output current i_o is positive, and the value of the current flowing through the inductor L_1 (i_{L1}) increases [28]. When operating in this mode, i_{bias}=- i_{L2}, and the voltage on L_1 is

$$L_1 \frac{di_{L1}}{dt} = \frac{1}{2}V_{DC} - Vg \tag{1}$$

ISSN: 2616 - 9916 | www.journalofbabylon.com | Journal.eng@uobabylon.edu.iq | info@journalofbabylon.com
مجلة جامعة بابل للعلوم الهندسية

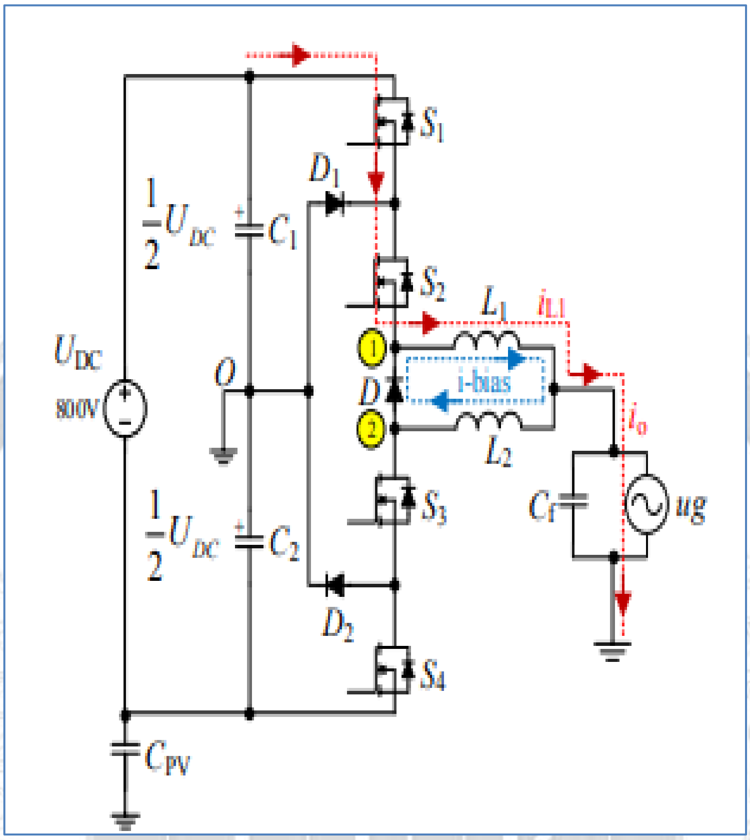

Figure 4. The Various Efforts of Operation: mode1 [28]

Mode 2 [Zero, level]: Figure (5) illustrates that the switch S_1 is turned off while the switch S_3 which is its complement is turned on. A positive output current ($i_o > 0$) turns D_1 ON connecting terminal (1) to the mid-point (O) by way of the connection between D_1 and S_2. Figure (5) shows that there is no voltage at the output of the bridge leg . During this time period the current through inductor L_1 is in the freewheeling stage which results in i_{L1} falling [28]. When operating in this mode, $i_{bias} = -i_{L2}$, and the voltage on L_1 is:

$$L_1 \frac{di_{L1}}{dt} = 0 - Vg \qquad (2)$$

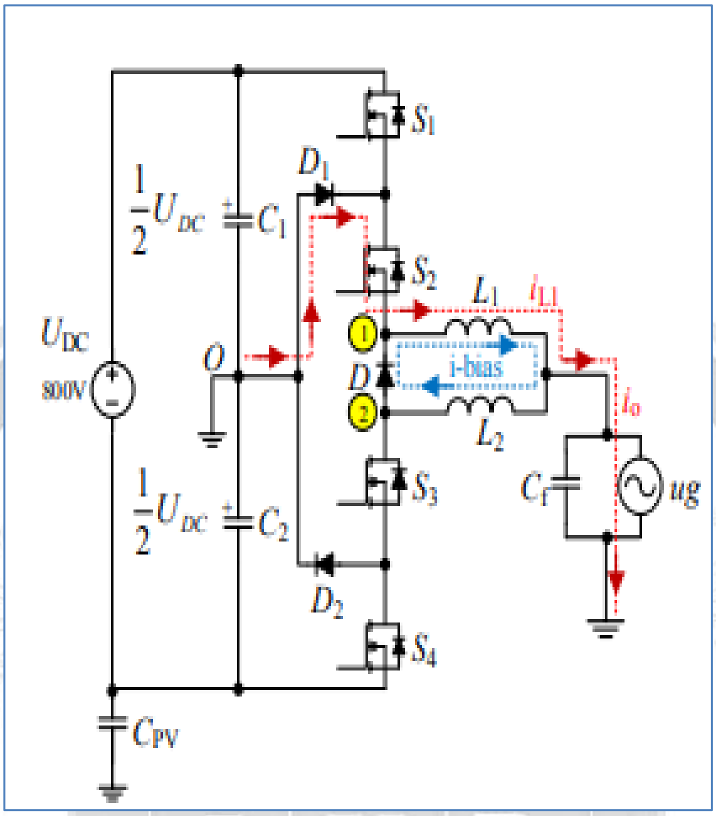

Figure 5. The Various Efforts of Operation: mode 2 [28]

Mode [Negative , $\frac{-Vdc}{2}$]: Figure (6) shows that switches (S_1 & S_4) are turned off while switch S_3 is on and switch S_2 is currently being turned off. In this scenario there is an abrupt drop in the voltage of V_1. Because of the induction potential of V_2 the parasitic body diode of S_4 will become active once its voltage drops below 1/2 V_{DC} and the body diodes of S_3 and S_4 all contribute to a linear reduction in the current at the circuit's conclusion. The value of capacitor C_2 stores the voltage of the negative half of the bridge hence its output is (-1/2) VDC . In this mode, $i_{bias} = - i_{L2}$.

ISSN: 2616 - 9916
www.journalofbabylon.com | Journal.eng@uobabylon.edu.iq | info@journalofbabylon.com

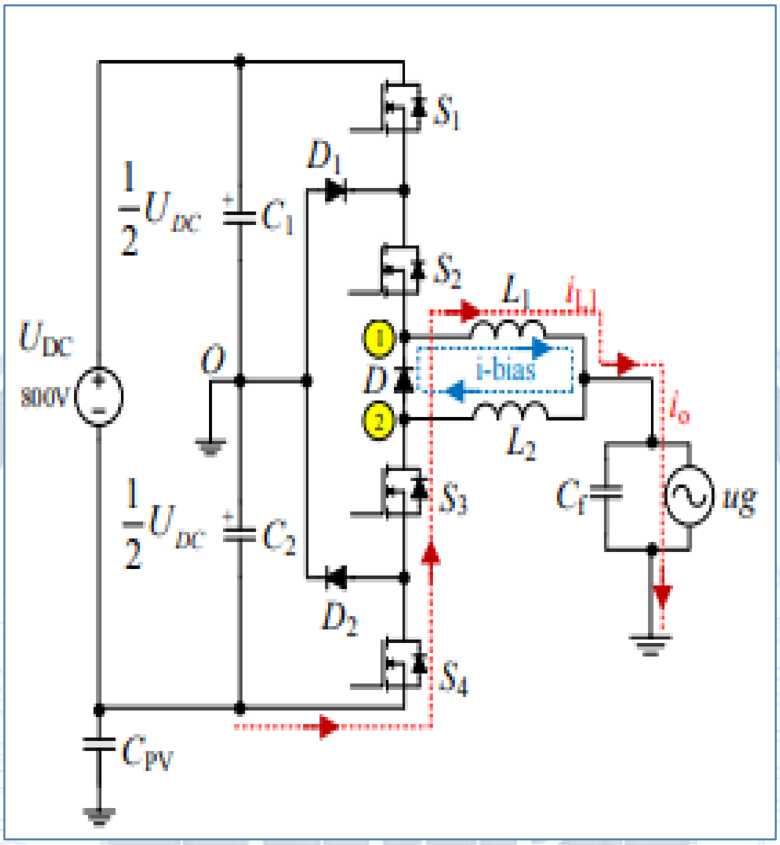

Figure 6. The Various Efforts of Operation: mode 3.[28]

III. Hysteresis current control

If the inverter has a unity power factor and the current through the inductor i_{L12} (the total current $I_{T=} I_{L1}+I_{L2}$), is synchronized with the grid voltage. This is necessary because a PV grid-connected inverter needs to keep the grid voltage and current at a unity power factor. However the current through the inductor must be consistently lowered to zero before the grid voltage drops below zero if the device is to operate safely. It is possible to precisely track the inductor current with the help of hysteresis current control. As can be seen in Figure (7) the inductor current should be zero before the grid voltage does (i.e inductor current should be zero at time xπ). Ideally the grid voltage should cross zero before the inductor current reaches zero. The following expression can be used to determine x, a period of time required to turn off high-frequency switching signals:

$$\frac{\int_{x\pi}^{\pi}[V_g \cdot \sin(\omega t)+V_D(\mathrm{ON})+V_S(\mathrm{ON})]}{L} \geq I_{\mathrm{ref}} \cdot \sin(x\pi)+\frac{h}{2} \quad (3)$$

This section contains the voltages while the power switches and clamping diodes are turned on. When they are both "on" these voltages are represented by their respective symbols V_D (on) and V_S (on). The high-frequency represented by the symbol x and the inductor current ripple also known as the bandwidth of the current hysteresis, is represented by the symbol h. [29] An efficient ways to implement hysteresis current control is through Hysteresis Band Real-Time Regulation, as it offers great performance a simple realization circuit, high stability and an inherent capability to limit current. This can be done by adjusting the hysteresis band.

$$h=\frac{V_g(V_{pv}-2 \cdot V_g)}{V_{pv} \cdot L \cdot f_s} \quad (4)\ [29]$$

Where:

ISSN: 2616 - 9916 | www.journalofbabylon.com | Journal.eng@uobabylon.edu.iq | info@journalofbabylon.com

f_s : stands for the expected switching frequency .
V_{pv}: voltage of photovoltaic system .
L: inductor .
Vg: grid voltage .

In addition, anti-islanding system may re-evaluate the amount of time it takes. The signals used for high-frequency switching are disabled. When the frequency of the measured voltage is rising in islanding mode, reaching the over-frequency limit requires decreasing time x via positive feedback. When the limit is reached, (i.e by increasing the gap of the current reference).

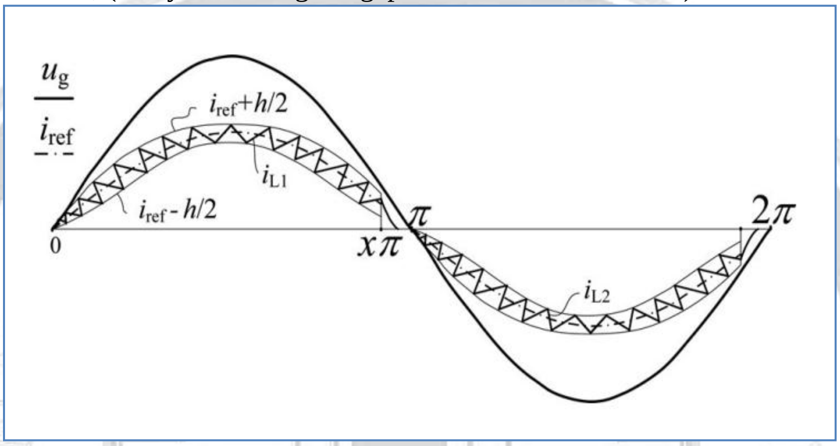

Figure 7. Phase control of inductor current i_{L12} .[29]

Implementing a hysteresis-current controller often entails the use of a closed-loop control system. A malfunction signal called e controls the inverter's switches. Symbolized by Iactual the inverter's error is the disparity between the actual current and the reference current Iref as shown in figure (8). Whenever the error rate rises over a predetermined limit transistors are switched limit the current they receive. As the error grows the current must rise since it has nowhere else to go. The hysteresis band refers to the range of the error signal which determines how much ripple there is in the inverter's output current. The two bounds that deal with deviations from the reference signal are known as the lower hysteresis limit and the upper hysteresis limit respectively. These boundaries are also known as the lower and upper hysteresis limits. The actual current remains within these limits regardless of changes a reference current.

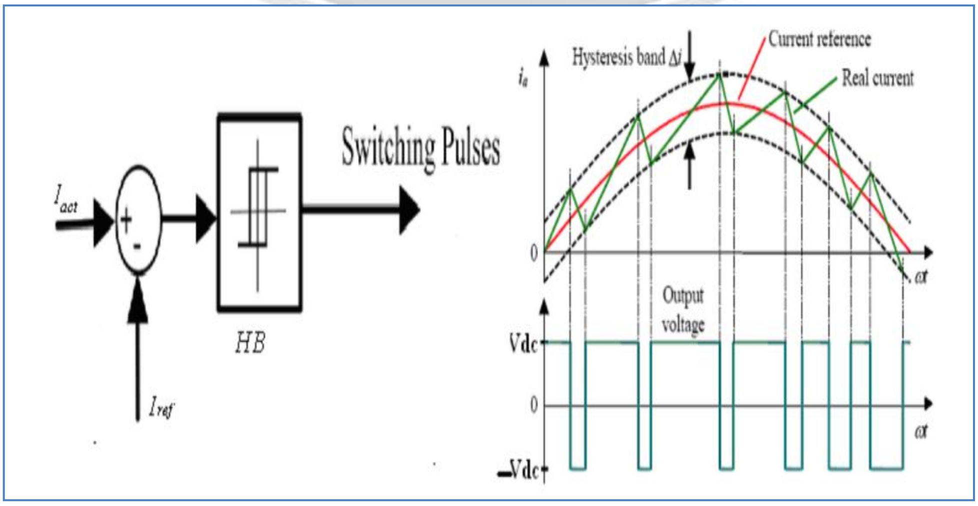

Figure 8. Hysteresis PWM Current Control and Switching logic.[29]

ISSN: 2616 - 9916 | www.journalofbabylon.com | Journal.eng@uobabylon.edu.iq | info@journalofbabylon.com

مـجلـة جـــامعة بـــابل للعلـــوم الهندسية مـجلـة جـــامعة بـــابل للعلـــوم الهندسية مـجلـة جـــامعة بـــابل للعلـــوم الهندسية

IV. Maximum Power Point Tracking (MPPT) Algorithms

The power value generated in PV systems varies depending on environmental factors. In PV panels, the system is required to work in MPP under all conditions. [18]Various MPPT algorithms are available for PV systems to operate MPP under variable environmental factors such as temperature and irradiance. MPPT algorithms used in this study are given as:

A. Perturb &Observe (P&O) Algorithm
B. Artificial Neural-Network (ANN) Algorithm

A. Perturb &Observe Algorithm

Perturb & Observe (P&O) algorithm is a frequently preferred MPPT method in PV applications due to its advantages such as having a simple structure, easy applicability and few parameters. The main working principle of P&O algorithm is basically based on the P-V characteristics of the PV panel. The operating current and voltage of the PV panel are measured instantly through sensors. The generated power value is calculated according to the measured current and voltage values. Power difference (ΔP) and voltage difference (ΔV) values are then observed by changing the operating voltage slightly in small steps. According to these values, the duty period rate is changed by (Δd) and MPPT is realized. [30] The procedure can be summarized as follows :

- If $\Delta P>0$ & $\Delta V > 0$, then duty period is reduced by Δd,
- If $\Delta P>0$ & $\Delta V < 0$, then duty period is increased by Δd,
- If $\Delta P< 0$, then duty period is increased by Δd,
- If ΔP 0, then duty period is reduced by Δd,

If the amount of change is zero, the algorithm returns to its initial step. The flow chart of the P&O algorithm figure 6 is also illustrated in Figure 9 [31].

ISSN: 2616 - 9916 | www.journalofbabylon.com | Journal.eng@uobabylon.edu.iq | info@journalofbabylon.com

مجلة جامعة بابل للعلوم الهندسية

ISSN: 2616 - 9916 | www.journalofbabylon.com | Journal.eng@uobabylon.edu.iq | info@journalofbabylon.com
مجلة جامعة بابل للعلوم الهندسية

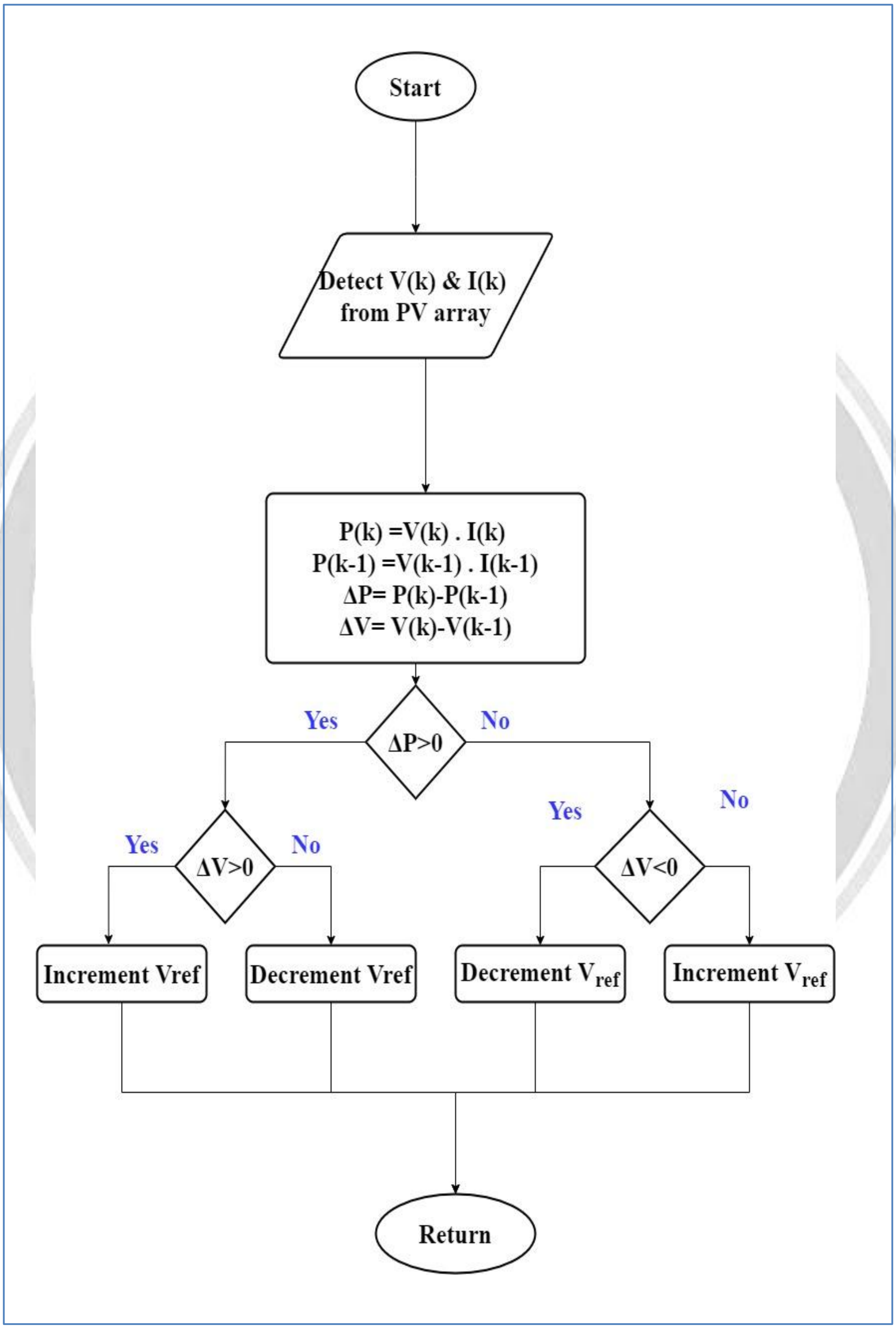

Figure 9. P&O Algorithm

B. Artificial Neural Network (ANN) Algorithm

ANN is an information processing technology inspired by the human brain's ability to learn. It generally consists of 5 sections , which are listed and described below as;

Inputs: Data sent to be collected in the neuron nucleus are called inputs.

Weights: To adjust the effect of inputs on the output, the connection they come from is multiplied by the weights and sent to the core.

Joining Function (NET): The function that calculates the net input of a cell is called the joining function. The sum of the inputs multiplied by their weights gives the net input function.

Activation Function: It is the part where the NET obtained in the combining function is sent to form the total cell output. When choosing the activation function the processing speed should be ensured to be easily differentiable.

Hidden layer: a layer in between input layers and output layers, where artificial neurons take in a set of weighted inputs and produce an output through an activation function.

Outputs: The value obtained as a result of the activation function expresses the output of the current neuron. Not only the values of the outputs are used as a result of ANN, but also they can be sent back to the network structure for further learning.

In order to make an accurate prediction of the voltage (V) or output power (P) at any given time, MPPT controllers make use of ANN. To figure out the load cycle the calculated value is put up against the instantaneous values that have been gathered. The temperature (T) and the irradiance (G) will both serve as examples of independent variables that will be used as **input variables** to the first layer of the network. Additional variables that are part of the panel such as V and I may be included as input. The processing of these information requests will be handled by the ten **hidden layers** [30-32]. The final performance will be determined by a number of factors including the activation function and training algorithm of chosen as well as the number of neurons in the hidden layers. It is recommended that a significant quantity of data be amassed for processing in order to further improve ANN's accuracy as shown in Figure (10)

ISSN: 2616 - 9916 | www.journalofbabylon.com | Journal.eng@uobabylon.edu.iq | info@journalofbabylon.com
مجلة جامعة بابل للعلوم الهندسية

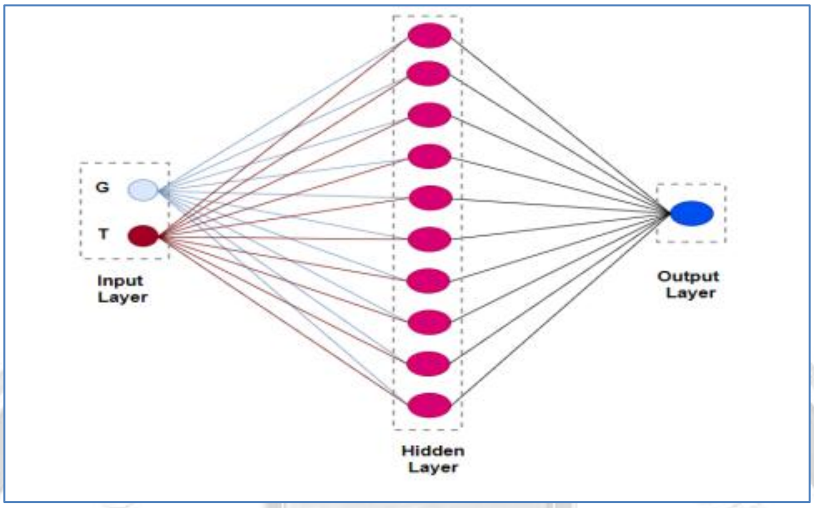

Figure 10. ANN Structure [32]

V. SIMULATION RESULT

In this section, the 3L-ISI-NPCI , MPPT , HCC and PLL has been designed and simulated using MatLab 2021a /SIMULINK environment a platform under MATLAB as shown in Figure (11) under standard condition performance of PV panel (Irr =1000 w/m^2 and T=25 ^{o}C). The converter behavior is examined under P&O and ANN MPPT algorithm only.

Figure 11. Simulink of PV system under P&O and ANN algorithms

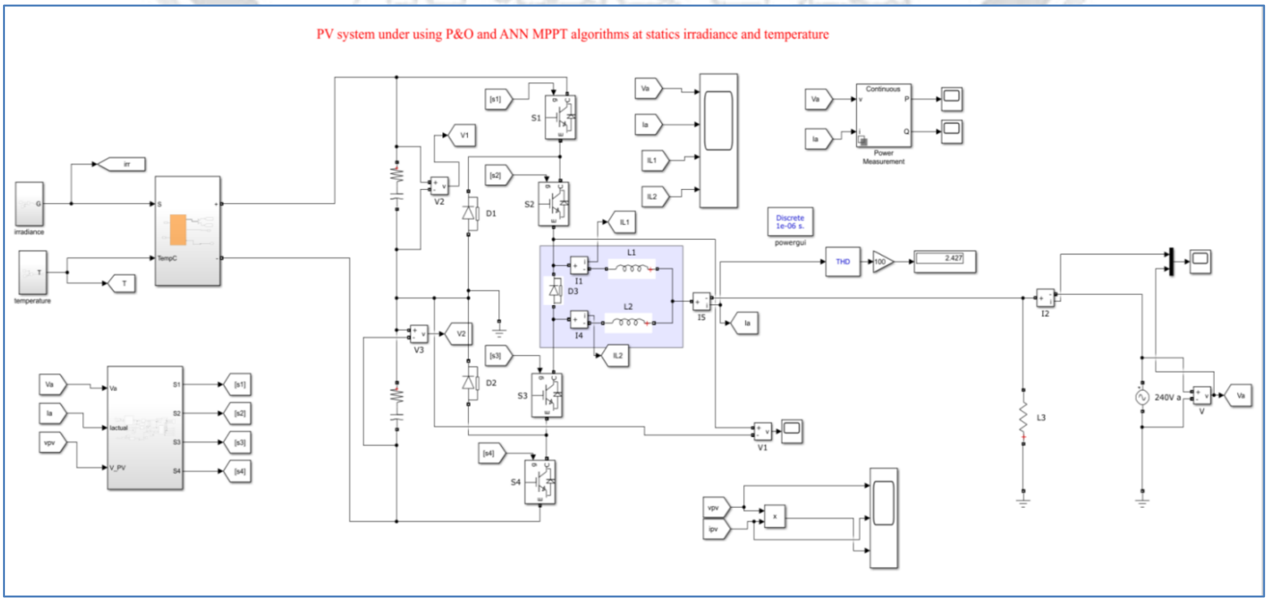

ISSN: 2616 - 9916 | www.journalofbabylon.com | Journal.eng@uobabylon.edu.iq | info@journalofbabylon.com

مجلة جامعة بابل للعلوم الهندسية

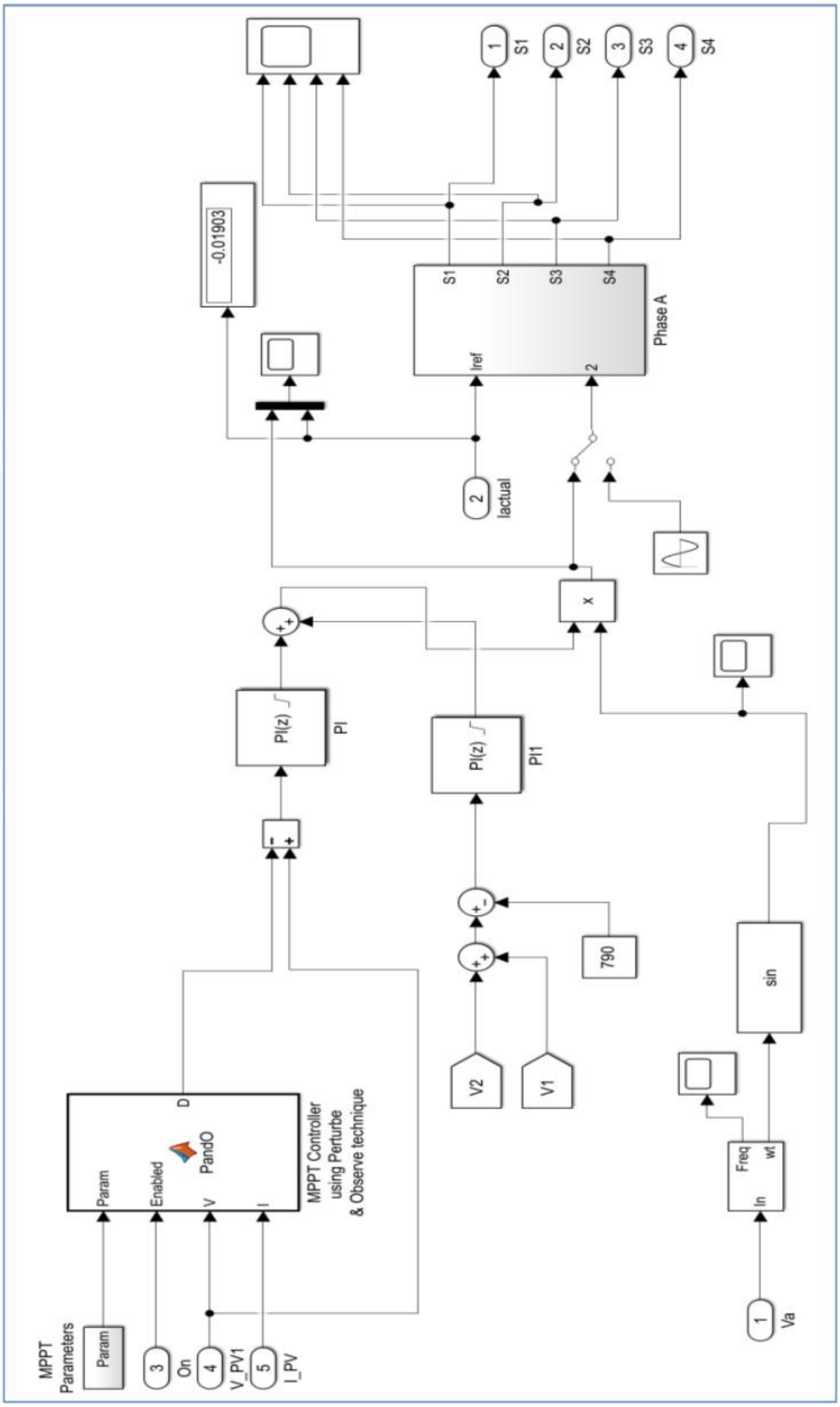

Figure 12. Simulink of controller with P&O algorithm.

info@journalofbabylon.com | Journal.eng@uobabylon.edu.iq | www.journalofbabylon.com ISSN: 2616 - 9916

ARTICLE
JOURNAL OF UNIVERSITY OF BABYLON
For ENGINEERING SCIENCES (JUBES)
Vol.31, No.3.| 2023

مجلة جامعة بابل للعلوم الهندسية

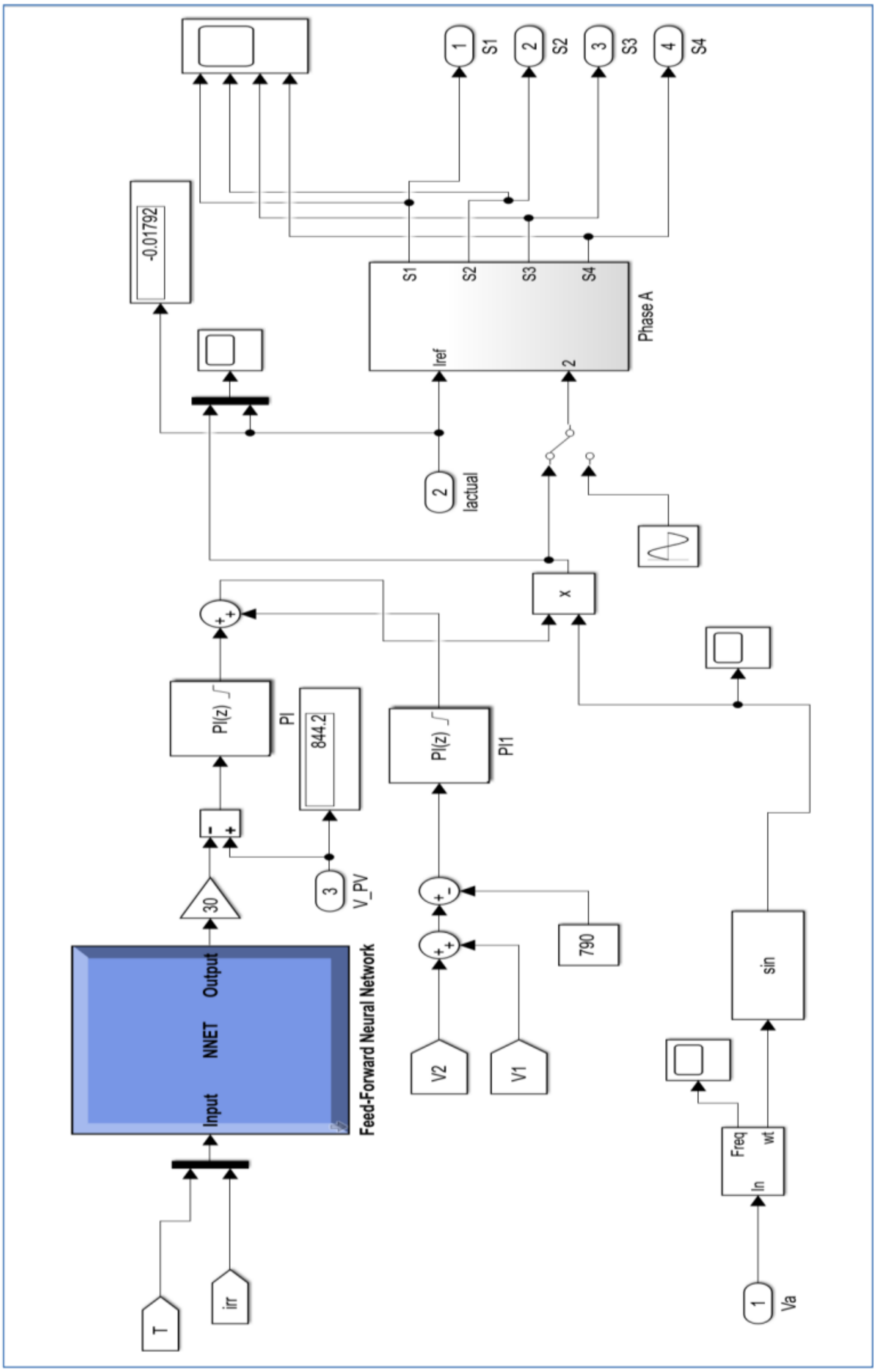

Figure 13. Simulink of controller with ANN algorithm

info@journalofbabylon.com | Journal.eng@uobabylon.edu.iq | www.journalofbabylon.com ISSN: 2616 - 9916

ISSN: 2616 - 9916
www.journalofbabylon.com | info@journalofbabylon.com | Journal.eng@uobabylon.edu.iq | www.journalofbabylon.com

The inductor currents (I, I_{l2}) and the output currents under different MPPT algorithims are shown in Fig.14. While Fig. 15 illustrates the three -level output voltage. Under both MPPT approaches, the Vpv, Ipv , P_{Pv}, Vc_1, V_{C2} are the same as shown in Figs 16-18. A sinusoidal grid voltage is shown in fig. 19, A lower current THD is achieved when using ANN algorithm with a value of 0.37 % as shown in figs 21.

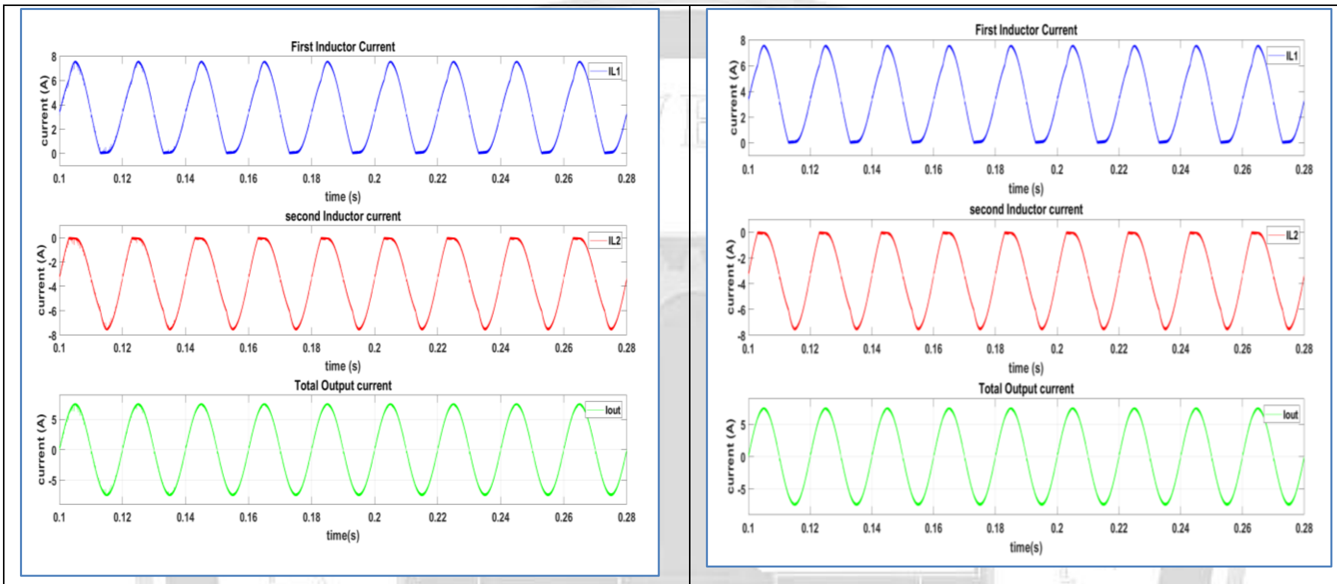

(a) (b)

Figure 14. I_{L1} , I_{L2} and I_{out} of 3 level ISI-NPC inverter under (a) P&O algorithm and (b) ANN algorithm

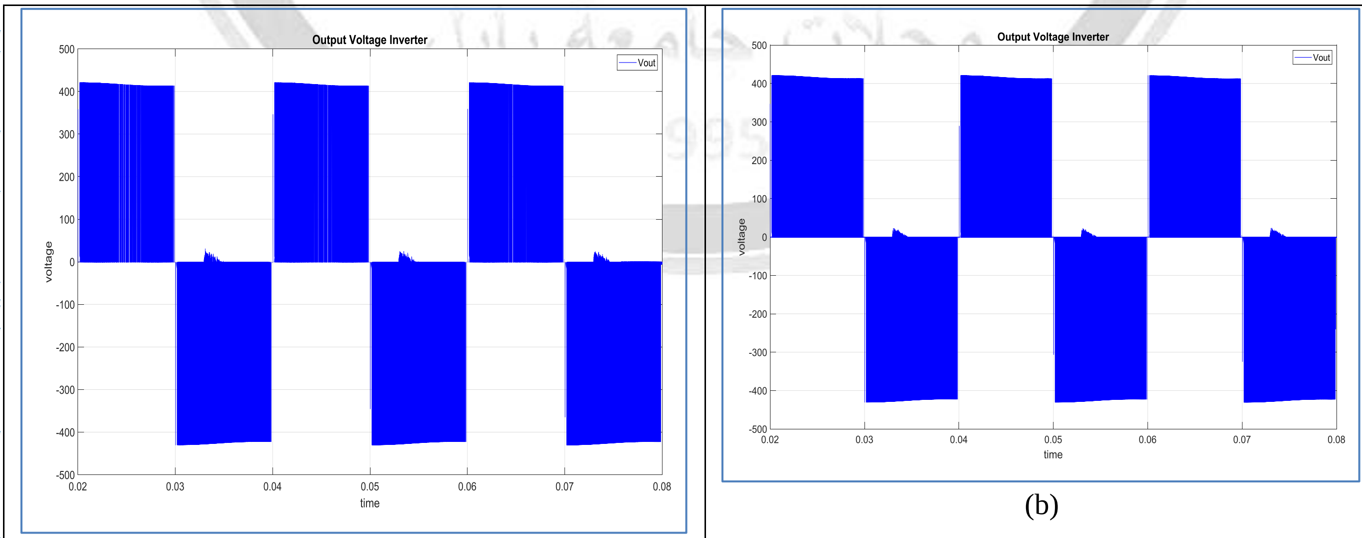

(a) (b)

Figure 15. Vout of 3 level ISI-NPC inverter under (a) P&O algorithm and (b) ANN algorithm

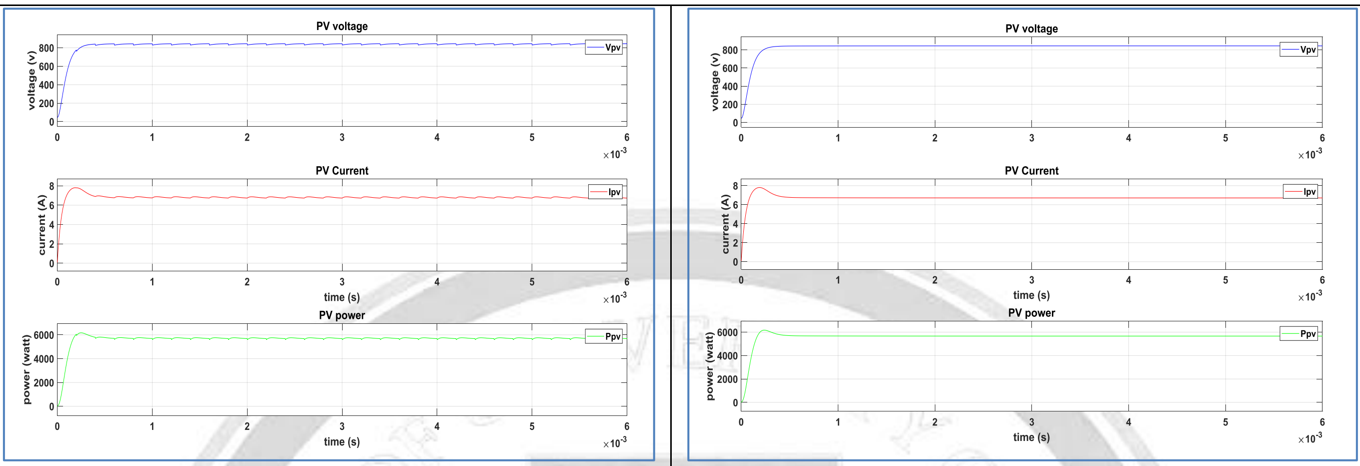

(a) (b)

Figure 16. **V_{PV}, I_{PV} and P_{PV} under (a) P&O algorithm and (b) ANN algorithm**

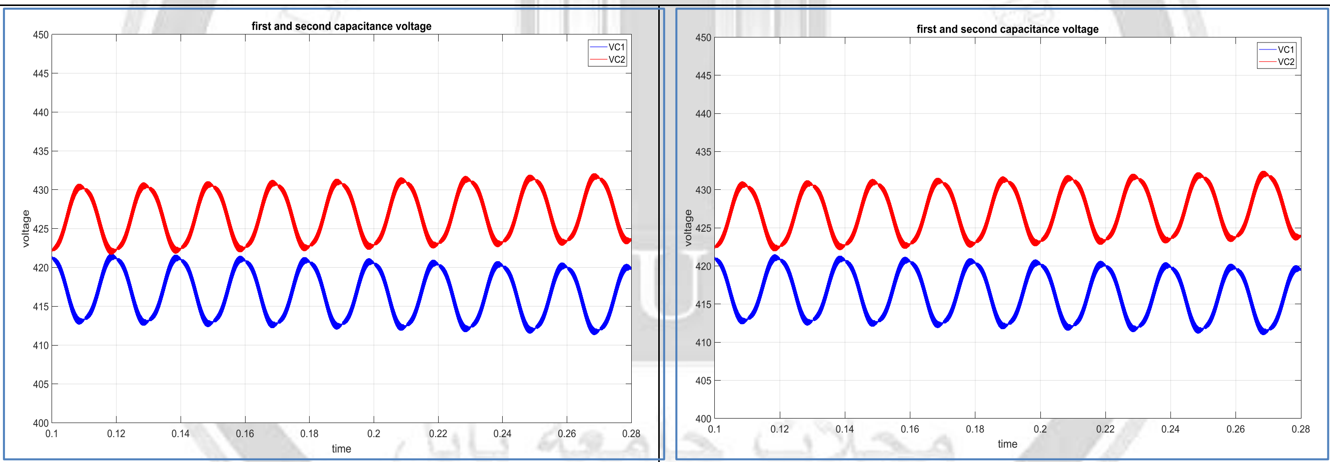

(a) (b)

Figure 17. **V_{C1} and V_{C2} of 3 level ISI-NPC inverter under (a) P&O algorithm and (b) ANN algorithm**

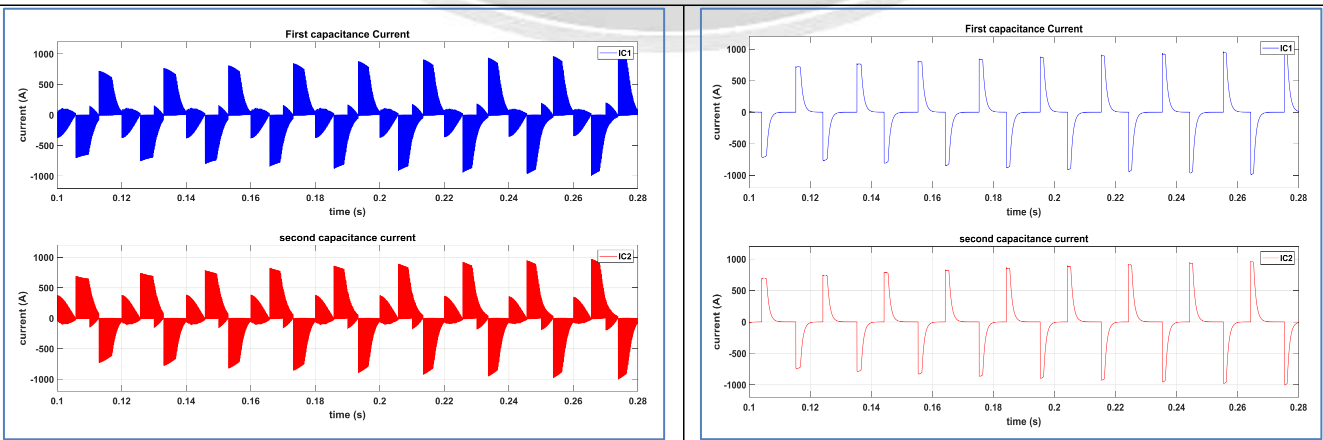

(a) (b)

Figure 18. **I_{C1} and I_{C2} of 3 level ISI-NPC inverter under (a) P&O algorithm and (b) ANN algorithm**

ISSN: 2616 - 9916 | www.journalofbabylon.com | Journal.eng@uobabylon.edu.iq | info@journalofbabylon.com

مجلة جامعة بابل للعلوم الهندسية

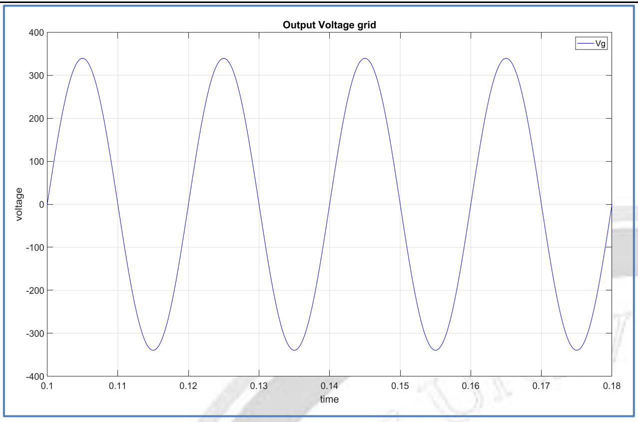

(a) (b)

Figure 19. V_{grid} under (a) P&O algorithm and (b) ANN algorithm

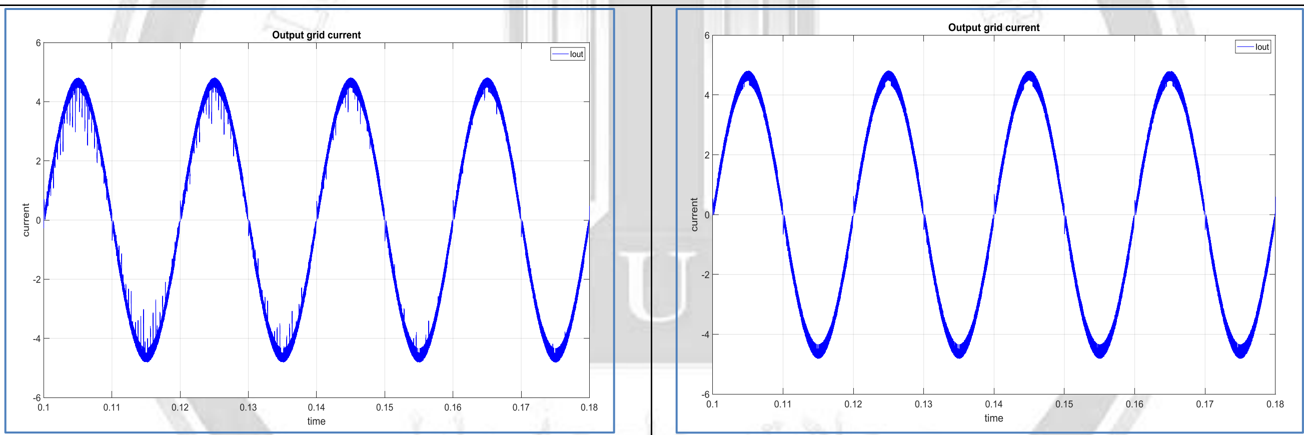

(a) (b)

Figure 20. I_{grid} under (a) P&O algorithm and (b) ANN algorithm

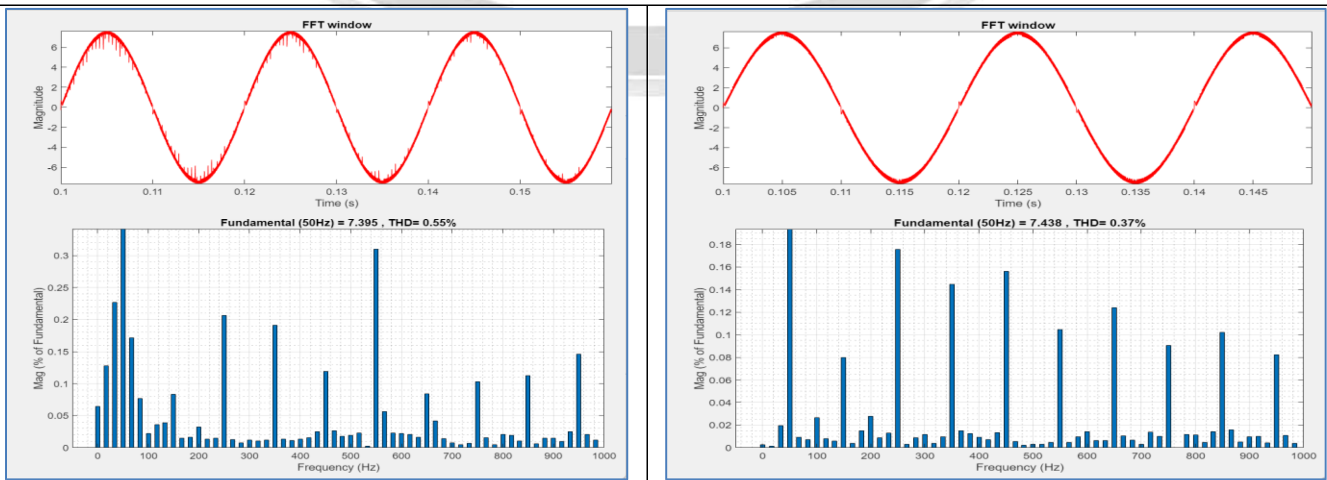

(a) (b)

Figure 21. FFT analysis of current THD under (a) P&O algorithm and (b) ANN algorithm

مجلــة جــامعة بــابل للعلـــوم الهندسية مجلــة جــامعة بــابل للعلـــوم الهندسية مجلــة جــامعة بــابل للعلـــوم الهندسية
ISSN: 2616 - 9916
www.journalofbabylon.com | Journal.eng@uobabylon.edu.iq | info@journalofbabylon.com

مـجلـة جـــامعة بــابـل للعلــــوم الهندسية
ISSN: 2616 - 9916 | www.journalofbabylon.com | Journal.eng@uobabylon.edu.iq | info@journalofbabylon.com

VI. CONCLUSIONS

In grid connected photovoltaic system, single-phase transformer-less multilevel inverters attract many researchers and industrial sectors due to their high efficiency, low cost, compact size, small volume and less complexity in comparison with galvanic isolation system (with transformer). However, the leakage current and shoot through issues are considered as a challenge in designing a transformer-less grid-connected PV system. In order to connect the PV generator to the power grid with no galvanic isolation, a powerful MLI needs to be proposed. A maximum power point tracking algorithm is essential to stabilise the DC output PV power by tracking its maximum point all day. The 3L ISI-NPC inverter is investigated to be employed in a grid connected PV system under two MPPT algorithm. A hysterisis current controller is used to maintain a good power quality of the utility grid with unity power factor. The results show that the 3L ISI-NPC inverter is able to integrate the PV system efficiently with the utility grid with no need to add dead time between switches and maintain unity power factor grid. By examining the converter operation under two MPPT algorithms, including P&O and Neural network, the results show that, applying the neural network algorithm with hysteresis current controller is more efficient than P&O algorithm. By adopting ANN algorithm, the current THD is reduced from 0.55% to 0.37 % .

REFERENCE

[1] F. Faraji, S. M. Mousavi G. A. Hajirayat, A. A. Motie Birjandi, and K. Al-Haddad, "Single-stage single-phase three-level neutral-point-clamped transformerless grid-connected photovoltaic inverters: topology review," ELSEVIER, Renewable and Sustainable Energy Review., vol. 80, pp. 197- 214, 2017.

[2] X. Guo, “A novel CH5 inverter for single-phase transformerless photovoltaic system applications,” IEEE Trans. Circuits and Systems II: Express Briefs, vol. 64, no. 10, pp. 1197-1201, 2017.

[3] S. A. Ahmed, M.S. Manoharan, and Joung-Hu Park “An efficient single sourced asymmetrical cascaded multilevel inverter with reduced leakage current suitable for single-stage PV systems,” IEEE Trans. Energy. Conv., vol. 34, no. 1, 2019.

[4] X. Guo, Y. Yang and T. Zhu, “ESI: A novel three-phase inverter with leakage current attenuation for transformerless PV systems," IEEE Trans. Ind. Electron., vol. 65, no. 4, pp. 2967-2974, Apr. 2018.

[5] E. Koutroulis, Y. Yang, and F. Blaabjerg, "Co-Design of the PV array and DC/AC inverter for maximizing the energy production in grid-connected applications," IEEE Trans. Energy. Conv., vol. 34, no. 1, 2019.

[6] X. Guo, B. We, T. Zhu, Z. Lu, L. Tan, X. Sun, and C. Zhang, “Leakage current suppression of three phase flying capacitor PV inverter with new carrier modulation and logic function,” IEEE Trans. Power Electron., vol. 33, no.3, pp. 2127-2135, Mar. 2018.

[7] X. Guo, X. Zhang, H. Guan, T. Kerekes, and F. Blaabjerg, “Three-Phase ZVR topology and modulation strategy for transformerless PV system,” IEEE Trans. Power. Electron., vol. 34, no. 2, pp. 1017-1021, 2019.

ISSN: 2616 - 9916 | www.journalofbabylon.com | Journal.eng@uobabylon.edu.iq | info@journalofbabylon.com

[8] X. Guo, J. Zhou, R. He, X. Jia, and Christian A. Rojas, "Leakage current attenuation of a three-phase cascaded inverter for transformerless gridconnected pv systems," IEEE Trans. Ind. Electron., vol. 65, no.1, pp. 676- 686, Jan. 2018.

[9] C. Yu, H. Xu, C. Liu, O. Wang, and X. Zhang, "Modeling and analysis of common-mode resonance in multi-parallel PV string inverters," IEEE Trans. Energy. Conv., vol. 34, no. 1, 2019.

[10] B. Mirfazel, "Survey of fault-tolerance techniques for three-phase voltage source inverters," IEEE Trans. Ind. Electron., vol. 61, no. 10, pp. 5192- 5202, Oct. 2014.

[11] B. Chen, P. Sun, C. Liu, C. Chen, J. Lai and W. Yu, "High efficiency transformerless photovoltaic inverter with wide-range power factor capability," Twenty-Seventh Annual IEEE Applied Power Electronics Conference and Exposition (APEC)., 2012. pp. 575-582.

[12] J. Salmon, Andrew M. Knight, and J. Ewanchuk, "Single-phase multilevel PWM inverter topologies using coupled inductors," IEEE Trans. Power. Electron., vol. 24, no. 5, pp. 1259-1266, May. 2009.

[13] N. R. Zargari, P. D. Ziogas, and G. Joos, "A two-switch high-performance current regulated DC/AC converter module," IEEE Trans. Ind. Appl., vol. 31, no. 3, pp. 583-589, May/Jun. 1995

[14] T. Markvart, 'Solar Electricity', John Wiley & Sons, Chichester, 1994.

[15] D. Rekioua , E. Matagne, Optimization of Photovoltaic Power Systems: Modelization, simulation and control , Springer Verlag London 2012.

[16] A. Safari and S. Mekhilef , " Incremental Conductance MPPT Method for PV Systems ", Electrical and Computer Engineering (CCECE), 2011 24th Canadian Conference on , pp. 345 - 347

[17] F. A. Inthamoussou , H.D. Battista, R. J. Mantz, "New concept in maximum power tracking for the control of a photovoltaic/hydrogen system" Int J Hydrogen Energy 2012; 37,pp 14951-14958.

[18] N. Femia, G. Petrone, G. Spagnuolo, and M. Vitelli, "A technique for improving P&O MPPT performances of double-stage grid-connected photovoltaic systems" ,IEEE Trans. Ind. Electron., vol. 56, no. 11,pp. 4473–4482, Nov. 2009.

[19] T. Esram and P. L. Chapman, "Comparison of photovoltaic array maximum power point tracking techniques" , IEEE Trans. Energy Convers., vol. 22, no. 2, pp. 439–449, Jun. 2007.

[20] G N. Femia, G. Petrone, G. Spagnuolo, M. Vitelli, "Optimization of perturb and observe maximum power point tracking method," IEEE Trans. Power Electron., vol. 20, no. 4, pp. 963–973, Jul. 2005.

[21] A. Safari, S. Mekhilef, "Simulation and hardware implementation of incremental conductance MPPT with direct control method using cuk converter" , IEEE Trans. Ind. Electron., vol. 58, no. 4, pp. 1154-1161, 2011.

[22] F. Liu, Y. Kang, Yu Zhang, Shanxu Duan, “Comparison of P&O and hill climbing MPPT methods for grid-connected PV converter” ,3rd IEEE Conference on Industrial Electronics and Applications, 2008 (ICIEA 2008), pp.804-807, 3-5 June 2008.

[23] S. Yuvarajan and S. Xuc, “Photo-voltaic power converter with a simple maximum-power-point-tracker,” in Proc. Int. Symp. Circuits Syst., 2003,pp. III-399–III-402.

[24] B. Bekker and H. J. Beukes, “Finding an optimal PV panel maximum power point tracking method,” in Proc. 7th AFRICON Conf. Africa, 2004, pp. 1125–1129.

[25] T. Hiyama, S. Kouzuma, T. Imakubo ,”Identification of optimal operating point of PV modules using neural network for real time maximum power tracking control”. IEEE Transactions on Energy Conversion 1995;10(2):360–7.

[26] Won C-Y, Kim D-H, Kim S-C, Kim W-S, Kim H-S. “A new maximum power point tracker of photovoltaic arrays using fuzzy controller”, In: Proc. 25th Annu. IEEE Power Electron. Spec. Conf.; 1994, pp. 396–403

[27] K. Punitha,a, D. Devaraj, a, S. Sakthivel Artificial neural network based modifed incremental conductance algorithm for maximum power point tracking in photovoltaic system under partial shading conditions, Energy 62 (2013) 330-340

[28] H. Xiao, and S. Xie, "Transformerless split-inductor neutral point clamped three-level PV grid-connected inverter," IEEE Trans. Power. Electron., vol. 27, no. 4, pp. 1799-1808, Apr. 2012

[29] M. Deepthi, “A Single-Phase Transformer less Inverter for Grid-Tied PV Applications by Using Hysteresis Controller”, IJRECE vol. 7 ISSUE 4 Oct.-Dec. 2019

[30] R. Ahmad, A. F. Murtaza, and H. A. Sher, “Power tracking techniques for efficient operation of photovoltaic array in solar applications – A review”, Renewable and Sustainable Energy Reviews, vol. 101. Elsevier Ltd, pp. 82–102, Mar. 01, 2019. doi: 10.1016/j.rser.2018.10.015

[31] N. Karami, N. Moubayed, and R. Outbib, “General review and classification of different MPPT Techniques”, Renewable and Sustainable Energy Reviews, vol. 68. Elsevier Ltd, pp. 1–18, Feb. 01, 2017. doi: 10.1016/j.rser.2016.09.132.

[32] M. YILMAZ and M. CORAPSİZ, “Artificial Neural Network based MPPT Algorithm with Boost Converter topology for Stand-Alone PV System”, *Erzincan Üniversitesi Fen Bilimleri Enstitüsü Dergisi*, vol. 15, no. 1, pp. 242–257, Mar. 2022, doi: 10.18185/erzifbed.1002823.

مجلة جامعة بابل للعلوم الهندسية

ISSN: 2616 - 9916 | www.journalofbabylon.com | Journal.eng@uobabylon.edu.iq | info@journalofbabylon.com

ARTICLE
JOURNAL OF UNIVERSITY OF BABYLON
For ENGINEERING SCIENCES (JUBES)
Vol.31, No.3.| 2023

محول أحادي الطور محسن متعدد المستويات بدون محول في ظل خوارزميات MPPT التقليدية والمتقدمة للتطبيقات الكهروضوئية

اسراء حسين الفتلاوي تهاني حمودي المهنا
قسم الهندسة الكهربائية/ جامعة بابل

esraa.hasson.engh306@student.uobabylon.edu.iq eng.tahany.hamodi@uobabylon.edu.iq

الخلاصة

يتم إدخال نظام كهروضوئي أحادي المرحلة بدون محول متصل بالشبكة مع عاكس متعدد المستويات، يتم استخدام العاكس متعدد المستويات لدمج النظام الكهروضوئي مع شبكة المرافق نظرًا لكفاءته العالية وتكلفته المنخفضة وصغر حجمه ووزنه ومع ذلك، فإن تيار التسرب بسبب عدم وجود عزل كلفاني هو أحد العوائق في مثل هذا النظام. تبحث هذه الورقة في عاكس أحادي الطور ثلاثي المستوى مثبت بنقطة محايدة ليتم استخدامه في نظام كهروضوئي أحادي المرحلة متصل بالشبكة. يتميز النظام بعامل القدرة الموحد والتشوه التوافقي الكلي للتيار المنخفض، والجهد المنخفض على مفاتيح أشباه الموصلات، وعدم إطلاق النار من خلال المشاكل، والموثوقية العالية والكفاءة. تقترح الورقة العاكس المحسّن ذو الحث المنقسم كمرشح فعال ليتم استخدامه في مثل هذا النظام الكهروضوئي الذي لا يحتوي على محول. تم تصميم التحكم في تيار التخلف لتتبع تيار خرج العاكس وإجباره على أن يكون صفراً من أجل تحقيق طاقة شبكة عالية الجودة والحفاظ على عامل طاقة الوحدة. يتم فحص خوارزميات تتبع الحد الأقصى من الطاقة التقليدية والمتقدمة بما في ذلك الاضطراب والمراقبة والشبكة العصبية الاصطناعية لضمان استخراج الطاقة القصوى من اللوحة الكهروضوئية. تم تصميم النظام بأكمله واختباره في هذا العمل. يتم تحقيق أداء أفضل في ظل نهج الشبكة العصبية الاصطناعية. تتحقق النتائج من قدرة العاكس المحسن ذو الحث المنقسم تحت التحكم في تيار التخلف والشبكة العصبية الاصطناعية لنقل الطاقة الكهروضوئية القصوى إلى الشبكة مع عامل طاقة موحد، وجودة طاقة عالية، وتيار منخفض للغاية تشوه متناسق كلي مع تبديل أشباه موصلات أقل بنسبة ٠.٣٧٪ الإجهاد، وبالتالي الموثوقية العالية لذلك، تسلط الورقة الضوء على أن العاكس المحسن ذو الحث المنقسم حيث تعتبر بمثابة عاكس متعدد المستويات فعالة ليتم استخدامها في مثل هذا النظام.

الكلمات الدالة: – نقطة محايدة مثبتة، نظام كهروضوئي، تحكم تيار التخلفية، خوارزمية اضطراب ومراقبة، شبكة عصبية اصطناعية، عاكس ، مرحلة واحدة ، متصل بالشبكة، أقصى تتبع لنقطة الطاقة.

ISSN: 2616 - 9916 | www.journalofbabylon.com | Journal.eng@uobabylon.edu.iq | info@journalofbabylon.com
مجلة جامعة بابل للعلوم الهندسية